ZKG INTERNATIONAL ISSN: 2366-1313

Enhancing the Brain Tissue Segmentation Kernelized Rough-Fuzzy C-Means method

[1]G.Rajasri, [2]A.Radhika

[1]Asst. Professor, Dep of CSE (Data Science), Geethanjali College of Engineering and Technology

[2]Asst.professor, Dep of CSE (E), Narsimha Reddy Engineering College, Maisamma guda.

[2]aarr00629@gmail.com

Abstract: *Brain magnetic resonance imaging (MRI) analysis is an exciting and ever-evolving field in biomedical engineering and artificial intelligence. Radiologists and other medical professionals can't advise on or implement the best course of therapy for anomalies like tumors or edoema unless they are detected early. Magnetic resonance imaging (MRI) offers numerous additional benefits as well as potential to be highly beneficial to medical practitioners. It has the potential to identify changes in several organs and tissues associated with illness by using a variety of magnetic resonance modalities (T1 weighted, T2 weighted, and T3 weighted) to provide very thorough scans of various brain regions. To be sure, a brain MRI might turn out different results if there are any anomalies, outliers, or background noise. Because of the potential for outliers and noise in brain MRI, traditional unsupervised machine learning approaches often provide segmentation results that are not correct. Furthermore, several brain components, such as cerebrospinal fluid (CSF), gray matter (GM), and white matter (WM), may be ambiguous, overlapping, complicated, and hard to understand in their most fundamental state. Additionally, there is no linear correlation between the tissue differentiability. Problems with standard unsupervised methods' outputs, inconsistencies in brain MRI datasets, sections of brain tissue that are hard to differentiate from one another owing to factors including noise, uncertainty, overlap, and indiscernibility, and non-linear separability of various brain tissue regions are the aims of this thesis.*

Keywords: Machine Learning, Prediction, Disease

I. INTRODUCTION

Brain magnetic resonance imaging (MRI) analysis is an exciting and ever-evolving field in biomedical engineering and artificial intelligence. Radiologists and other medical professionals can't advise on or implement the best course of therapy for anomalies like tumors or edoema unless they are detected early. Magnetic resonance imaging (MRI) offers numerous additional benefits as well as potential to be highly beneficial to medical practitioners. It has the potential to identify changes in several organs and tissues associated with illness by using a variety of magnetic resonance modalities (T1 weighted, T2 weighted, and T3 weighted) to provide very thorough scans of various brain regions. To be sure, a brain MRI might turn out different results if there are any anomalies, outliers, or background noise. Because of the potential for outliers and noise in brain MRI, traditional unsupervised machine learning approaches often provide segmentation results that are not correct. Furthermore, several brain components, such as cerebrospinal fluid (CSF), gray matter (GM), and white matter (WM), may be ambiguous, overlapping, complicated, and hard to understand in their most fundamental state. Additionally, there is no linear correlation between the tissue differentiability. Problems with standard unsupervised methods' outputs, inconsistencies in brain MRI datasets, sections of brain tissue that are hard to differentiate from one another owing to factors including noise, uncertainty, overlap, and indiscernibility, and non-linear separability of various brain tissue regions are the aims of this paper.

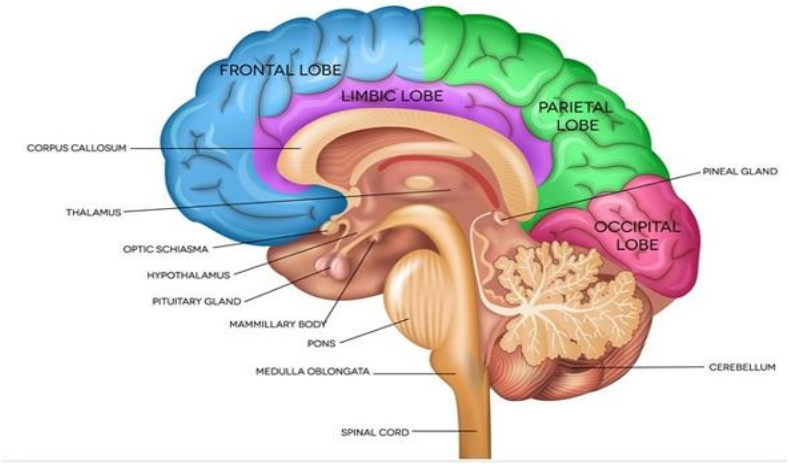

Figure 1.1: Anatomy of human Brain

The cerebral cortex is located on the cerebral periphery. There are many hills and valleys in its structure, and there are about 16 billion neurons in certain levels. Figure 1.3 shows the

typical brain perspective. Every fold in the brain is defined by a gyrus, and every groove between two folds is defined by a sulcus. The distinctive grey-brown hue of the cortex is imparted by the cell bodies of gray matter (GM). On the flip side, white matters (WM) are lengthy nerve cells that link various parts of the brain. On the other hand, cerebrospinal fluid (CSF) is colorless and transparent and fills the brain's cavities. Cerebrospinal fluid (CSF) does more than only cushion the brain from impact; it also nourishes the blood by delivering nutrients like glucose and oxygen. The WM is the primary pathway for signals to go between the left and right cerebral hemispheres. Several higher-level tasks are within the GM's purview, including language, memory, learning, and conscious perception.

Three possible 3D brain cross-sections are shown in Figure 1.4: the axial/transversal, sagittal, and coronal perspectives. Because it lacks depth, a plane is like a specter penetrating a three-dimensional brain. The fields of anatomy and medical research often address these three perspectives on planning. These stand for different schools of thought about the anatomy of the brain.

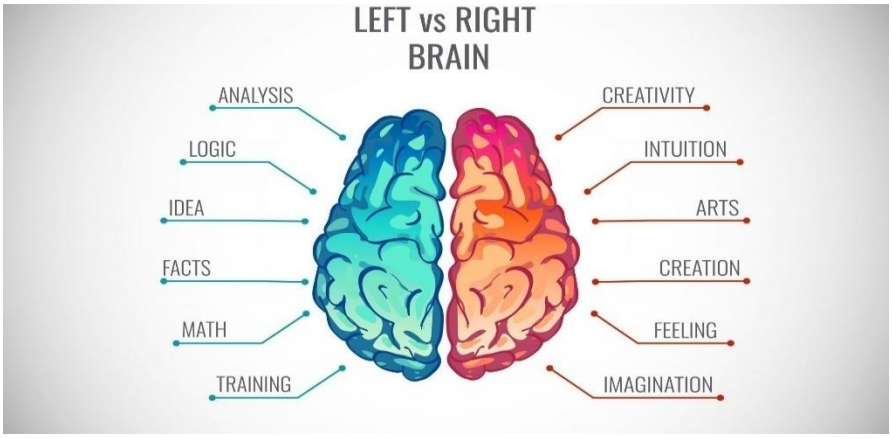

Figure 1.2: left and right hemisphere of human brain

The coronal plane, also called the frontal plane, is a vertical slice across the middle of the brain when seen in a sagittal plane. It separates the front and posterior regions of the brain.

The cerebral hemispheres are vertically divided along a sagittal line that is perpendicular to the coronal plane. From above or below: The axial plane, which is sometimes called the horizontal plane, divides the brain into the upper and lower halves. It runs perpendicular to the sagittal and coronal planes. When the brain is in an upright position, its axial plane will lie perpendicular to the floor. According to references [1, 3, 4], cross sections are generated

by the transverse planes. A wide variety of problems may arise due to brain abnormalities. Here you can find descriptions of the most common brain disorders that people suffer from. Brain neoplasms, sometimes known as tumors, are dangerous, uncontrolled cell growths in the brain [7, 8]. Brain tumors come in a wide variety of forms, from benign to malignant. Brain tumors, also known as malignant tumors or secondary or metastatic tumors, may spread from other parts of the body and pose a serious health risk. Malignant brain tumors spread to other parts of the body and cause more damage than benign brain tumors, which are also known as primary brain tumors [7-9]. Classification of brain tumors into classes I, II, III, and IV is based mostly on their severity [7, 10]. Microscopic examination reveals that grade I brain tumor cells seem to be almost normal. They are the safest, take the longest to develop, and are often associated with increased longevity. Surgery may be effective in removing an I grade brain tumor. Grade I brain tumors include gangliocytomas and gangliogliomas [10]. Grade II brain tumors progress moderately, sometimes metastasize (spread to other organs), and have cells that seem slightly abnormal under a microscope. A grade III brain tumor is characterized by its aggressiveness, rapid proliferation of abnormal cells, and likelihood of progressing to a grade IV tumor. Anaplastic astrocytoma is one kind of grade III brain cancer. The most dangerous sort of brain tumor is a grade IV tumor. Dead cells accumulate into the core of grade IV tumor cells. The rapid growth, fast rate of replication, and potential infiltration of neighboring cells define this tumor type. It encourages angiogenesis, the process by which new blood vessels are formed, to sustain its continuous growth. The grade IV brain tumor known as glioblastoma (GBM) may also be termed malignant astrocytic glioma.

Dementia is mostly caused by Alzheimer's disease (AD) and other associated illnesses [13]. The gradual loss of cognitive function is caused by the continual and permanent destruction to brain cells in this chronic neurodegenerative condition. Everyday cognitive skills including independent remembering, thinking, and reasoning become more challenging for people with this illness [10]. Memory loss for recent conversations or occurrences is one of the early warning indicators of Alzheimer's disease. Eventually, a person with Alzheimer's may lose the ability to do routine chores and their most meaningful memories may start to vanish. Deterioration of cognitive abilities may lead to fatal outcomes in more serious instances [8-9]. In many cases, the first symptoms of Alzheimer's disease manifest in a person's youth, often around the 1960s.

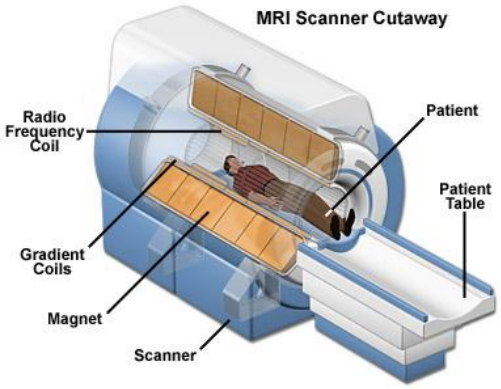

Figure 1.3: MRI Scanner

II. Literature Survey

Diagnostic imaging technologies include computer tomography (CT), X-ray, radioactive tomography (RA), and magnetic resonance imaging (MRI). Among the several medical imaging techniques, magnetic resonance imaging (MRI) has the potential to be the gold standard for diagnosing abnormalities in organs and tissues at an early stage. Among the most crucial applications of magnetic resonance imaging (MRI) technology is brain imaging. Radio waves and a magnetic field are used in this non-invasive technique to provide precise pictures of the brain and brain stem [28]. It is possible to create multimodal imaging of tissues with varying contrasts by combining MRI images weighted in T1, T2, and PD (proton density) [19, 28, 31]. Accurate segmentation is crucial for detecting tumors, edoema, necrotic tissues, and other abnormalities in the brain's intricate structure. Clinical examination of chemicals, odd anatomical locations, and morphological features used to be the gold standard for detecting these disorders.

It is reported that the K-Means clustering approach has a lower execution time than FCM clustering, and the tumor area has been computed for some reliable results. Since fuzzy C Means is a semi-supervised method, the K-Means clustering strategy yielded better results. There is no requirement for pre-processing with K-Means Clustering since it is an unsupervised approach with fewer repetitions. K-Means Clustering provides the best lossless compression. Precise findings were also established with a little quantity of data. Using the K-means method, Sanghamitra T. Kamble and colleagues (2015) demonstrated a variety of malignancies and their extraction from encephalon cells. The "k-means" technique and tumor both need input images that are devoid of noise.

Ranjana R. In order to distribute photos, segmenting medical images is crucial since it removes suspicious areas (et al., 2015). A cancer detection approach for brain MRI image segmentation based on K-Means clustering has been suggested by them.

To classify brain tumors, Santhosh Rishnan et al. (2016) utilize ANFIS; to divide images and use artificial neural fuzzy skills; to remove characteristics needed to detect malignancies in images, they use GLCM; and to reduce noise, they use median filter. Brain abnormalities were identified and the kind of brain cancer was identified via the use of magnetic resonance imaging (MRI). Before looking at feature extraction methods, medical pictures are subjected to a slew of image pre-processing techniques. Next, the images are partitioned to separate brain tumors from the rest of the image.

Medical image inquiry might be substantially enhanced by the evaluation criteria proposed by Zhongyu Li and colleagues (2017), which include a range of investigative and diagnostic scenarios, with the goal of facilitating large-scale retrieval. This method for detecting brain tumors developed by T. In order to determine the tumor's dimensions inside a segmented region, Sathies Kumar and colleagues (2017) used a "SVM Classifier" in conjunction with segmentation. In order to determine the kind of tumor, an artificial neural network will be trained utilizing the retrieved attributes of the segmented section. This enables the localization of an aberrant cell mass inside a specific MRI slice.

According to Emre Dandi and colleagues (2017), this is the first motivation for creating user-interface software. So, the responsible doctors' case will be covered. This means the application software is less likely to make mistakes, which might lead to its eventual use as a wearable tool for extra brain tumor segmentation. The suggested application has the potential to detect brain cancers, according to extensive test studies conducted on picture datasets.

III. Proposed Methodology

Because of its diagnostic use, imaging technology is crucial to biomedical engineering. The field of medical imaging technology offers a wide variety of diagnostic instruments, such as X-rays, CT, MRI, and PET. When it comes to diagnosing changes in organs and tissues, magnetic resonance imaging (MRI) is among the most popular and effective tools in the toolbox. A popular and useful diagnostic tool, magnetic resonance imaging (MRI) uses radio waves and a magnetic field to create high-resolution images of the brain and its inner

structures. Brain magnetic resonance imaging (MRI) is a common diagnostic technique. T1, T2, and PD (proton density) weighted MRI techniques may be used in brain MRI to get multimodal pictures of tissues with varying contrasts.

Improving Rough Fuzzy C-Means for The Segmentation of Brain Tissues based on Their Environment

After extending the kernel trick idea, spatial restrictions were used to enhance and modify rough-fuzzy clustering. The purpose of this was to respond to the concerns voiced in the introduction on the lack of background information. Complex brain (MRI) tissue sections are notoriously difficult to segment because to their inherent ambiguity, noise, overlapping, and normal conditional difficulties. This method is predicted to provide accurate segmentation in such cases.

This data pattern (pixels) xk and the cluster center (vi) may be projected onto a higher dimensional space using the kernel approach. Compared to the previous space, this one has a much greater chance of cluster separation due to a linear barrier. The kernel approach is used to execute a non-linear adjustment on the input data points using a Mercer kernel. The purpose of this operation is to map the points of data onto a feature space with several dimensions. Therefore, the original kernel concept increases the probability that complex regions that were not linearly separable in the feature space will be so when applied in its current version.

The non-linear transformation done to a data point so that it may be projected onto a higher dimensional feature space is denoted by the symbol. The inner product of $\varphi(\vec{x}_i)$ and $\varphi(\vec{y}_i)$ [126] is the kernel function $K(\vec{x}_i , \vec{y}_i) = \varphi(\vec{x}_i)\ T\ \varphi(\vec{y}_i)$. The radial basis function (RBF) generally used for kernel is: $K(\vec{x}_i , \vec{y}_i) = \varphi(\vec{x}_i)\ T\ \varphi(\vec{y}_i)$ [127]

$$\mathbb{K}(\vec{x}_i, \vec{y}_i) = \exp\left(\frac{\left(-\sum_{i=1}^{d} |\vec{x}_i - \vec{y}_i|^a\right)^b}{\sigma^2}\right) \text{---------} (3.1)$$

Where d indicates the dimension (feature) of the data collection; and is equal to zero; 1 is equal to one; and 2 is equal to two. Because of the kernel trick [89, 102, 103], the Euclidian distance is replaced with the kernel distance $\mathbb{K}(\vec{x}_k, \vec{v}_i)$, resulting in the kernelized fuzzy objective function JKFCM, as described in Equation (3.2):

$$J_{KFCM} = 2\sum_{i=1}^{C}\sum_{k=1}^{N}\mu_{ik}^{m}\left(1-\mathbb{K}(\vec{x}_k,\vec{v}_i)\right) \text{----------} (3.2)$$

Because of this, the membership function (μ_{ik}) and the cluster centres ($\vec{v}_i$) are changed in the following ways.

$$\mu_{ik} = \frac{\left(1-\mathbb{K}(\vec{x}_k,\vec{v}_i)\right)^{\frac{1}{1-m}}}{\sum_{i=1}^{C}\left(1-\mathbb{K}(\vec{x}_k,\vec{v}_i)\right)^{\frac{1}{1-m}}} \text{----------} (3.3)$$

$$\vec{v}_i = \frac{\sum_{k=1}^{N}\mu_{ik}^{m}\mathbb{K}(\vec{x}_k,\vec{v}_i)\vec{x}_k}{\sum_{k=1}^{N}\mu_{ik}^{m}\mathbb{K}(\vec{x}_k,\vec{v}_i)} \text{----------} (3.4)$$

When the total number of clusters is represented by C, and the total number of pixels is represented by N, the fuzziness index is denoted by the letter m, and one m is equal to the total number of pixels. In order to address the problems caused by noise and artefacts, spatial contextual information has been further incorporated into the clustering process (in Equation 3.2). This has made it possible for the pixel labels to be influenced by the effect of the pixels that are immediately adjacent to them, which is expected to produce good segmentation results. in order to deal with these issues. Once spatial contextual information is included, a rewrite of the objective function JKF CM (in Equation 3.2) may be achieved, as shown in Equation 3. (3.5)

$$J_{KFCMSC} = \sum_{i=1}^{C}\sum_{k=1}^{N}\mu_{ik}^{m}\left(1-\mathbb{K}(\vec{x}_k,\vec{v}_i)\right) + \alpha\sum_{i=1}^{C}\sum_{k=1}^{N}\mu_{ik}^{m}\left(1-\mathbb{K}(\vec{x}_k,\vec{v}_i)\right) \text{---} (3.6)$$

A tiny window (usually 33 or 55) is used to indicate the mean or median of the near adjacent pixels (i.e., those that are present in a short window around the pixel of interest). Two parts of Equation (3.5) are involved, with the first part being directly associated with and borrowed from the standard Fuzzy C-Means (FCM) types algorithm with kernel, and the second part being in charge of computing the mean or median immediate neighbouring pixels around any given pixel xk, which aids in dealing with noise or outliers present in the image and is intended to improve performance segmentation method. The mean filtering or median filtering approach (in this case, the mean value for x e k) may be used to calculate x e k in advance, as opposed to [97], and the controlling parameter, which governs the influence of

the surrounding term, is utilised in the current study. In cases This method is identical to standard KFCM when either or is zero or infinite.

Algorithm: Kernelized Rough – Fuzzy

Input: Set of pixels $\vec{x}_k$ present in the image, number of clusters C, and user defined parameters $(m, \alpha$, threshold, and $w_{low})$.

Output: Set of segmented pixels (in the form segmented image).

Method:

1: Mean vector $\vec{x}_k(\forall k)$ is computed in advance for the neighbouring pixels within a small window centering around $\vec{x}_k$.

2: Cluster centers $\vec{v}_i, \forall i = 1$ to C are assigned randomly in the initial stage.

3: while (not convergence) do

4: Memberships μ_{ik} is computed by using Equation (3.6) for all clusters C and all pixels N.

5: for each pixel $\vec{x}_k, k = 1: N$ do

6: Assign the maximum membership grade for pixel $\vec{x}_k$ as follows:

$$\mu_{pk} \leftarrow \max_{j=1:C}(\mu_{jk}),$$

$$\text{where, } p = \text{argmax}$$

7: for $j = 1: C$ and $j \neq p$ do

8: if $\mu_{jk}/\mu_{pk} >$ threshold then

9: $\vec{x}_k$ is assigned to the upper approximations $\bar{B}X_j$ and $\bar{B}X_p$.

10: end if

11: end for

12: if $\vec{x}_k \notin$ any upper approximation then

13: if $\vec{x}_k \notin$

14: $\vec{x}_k$ is

end if

15: end for

16: Cluster centers $\vec{v}_i, \forall i = 1: C$ are updated based on Equation (3.13).

17: end while

MRI segmentation relies on partitive clustering, therefore pixels must be assigned to clusters until convergence. We cease (re)assigning pixels when the clustering process has converged and cluster centers have not changed between rounds. The well-known Gauss-Seidel

algorithm may converge the suggested technique [48]. Gauss-Seidel converges when the confusion matrix (CM) has only diagonally dominating equations. Confusion matrices (CMs) represent the technique as equations. The pixels given to each cluster at each step may be used to create a confusion matrix Mcc of size C x C (where C is the number of clusters). If the CM is diagonally dominating, the clustering algorithm has converged; otherwise, it may not have. When the diagonal elements in each row of the CM are more than zero and the off-diagonal elements are zero or fewer, it will converge.

IV. Experimental Evaluation

MRI datasets used

We conduct tests using a variety of genuine and generated benchmark MRI datasets, both with and without noise, as well as BrainWeb and IBSR image databases. The IBSR dataset is genuine data, however BrainWeb is synthetic. One MRI brain scan typically has four clusters: white matter (WM), grey matter (GM), cerebrospinal fluid (CSF), and backdrop. These clusters assess critical brain areas' relevance. The BrainWeb images are (217 x 181), whereas the IBSR image is (128 x 256). This study looked at T1 and T2 weighted modalities. Figure 3.1 displays BrainWeb MRI datasets for several planes and modalities. T1 and T2 weighted modalities for the Z85, Z93, Z95, and Z100 planes are shown in the photos. Figure 3.2 shows typical Z85 ground truth shots. The database provides ground facts for each segment by designating the pixel in the segment with the largest fuzzy membership based on the major brain portion (white matter, grey matter, and CSF). The pictures' dark backgrounds indicate the absence of smaller brain areas. Common IBSR datasets include IBSR144, IBSR150, IBSR155, and IBSR167, each with ground facts.

Jaccard coefficient

The ratio of the pixels that are shared by both the original (L) and segmented (M) image to that of the united function (or the collection of pixels shared between images that are input (L) and segmented (M) image) can be described as the intersection (IOU) coefficient (M). This implies that the summation function (S) represents an intersection between the values for pixel in the image input (L) as well as the image segmented (M) and there is the Jaccard coefficient (J) is the ratio of the intersection and union of these two values (M).

ISSN: 2366-1313

$$J(L, M) = \frac{S(L \cap M)}{S(L \cup M)}$$

The better the segmentation, the higher the value of the Jaccard coefficient. The Jaccard coefficient has a range of 0 to 1, with a maximum of 1. The closer the value of Jaccard comes to one, the better the performance.

Dice coefficient (DC)

Dice coefficient value is stated using the Jaccard index J. (L, M). DC is a function that can be written as where L is the input image and M is the segmented output image:

$$D(L, M) = 2 \times \frac{J(L, M)}{1 + J(L, M)}$$

The highest value of the Dice coefficient is 1, with the range being from 0 to 1. The closer the value of Dice is to one, the better the segmentation.

Kernelized Xie-Beni Index (KXBI)

It's an unsupervised measure for measuring cluster validity. Each cluster's intra-cluster compactness is measured by calculating the average square distance between each pixel and the cluster's centre, while the inter-cluster separation is the lowest square distance between the clusters' centres (or clusters). A lower KXBI number indicates a better-quality cluster. The KXBI may take on values between 0 and 1, with 1 being its maximum. For those interested, the Xie-Beni index after kernelization is defined as:

$$KXBI = \frac{2 \times \sum_{k=1}^{n} \left\{ \sum_{j=1}^{c} \left(1 - \mathbb{K}(\vec{x}_k, \vec{v}_j)^{\frac{1}{1-m}} \right)^{(1-m)} \right\}}{n \times \min_{i \neq j} \left[2 \times \left\{ 1 - \mathbb{K}(\vec{v}_i, \vec{v}_j) \right\} \right]}$$

Increased segmentation lowers kernelized Xie-Beni index. Kerneled Xie-Beni index is 0–1 with a maximum of 1.

Finally, compares SEKRFC's ground truths and segmented outputs to clustering-based techniques for a brain MRI Z100 plane with 6% "salt and pepper" noise. Different figures show typical segmented picture findings for different locations. Figure 3.10 shows that only SEKRFC can identify all segments with low background noise. Grey matter matters, but no other approach can identify it. The trials matched brain MRIs. SEKRFC outperforms

clustering-based segmentation on whole brain MRI. Image segmentation clarity and validity indices show this. The "salt and pepper" and "Rician" method of picture segmentation sounds superior.

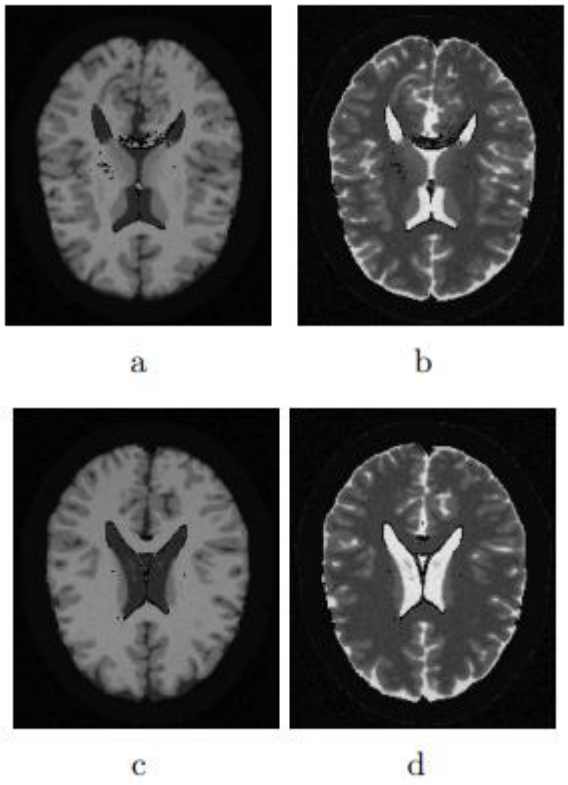

ISSN: 2366-1313

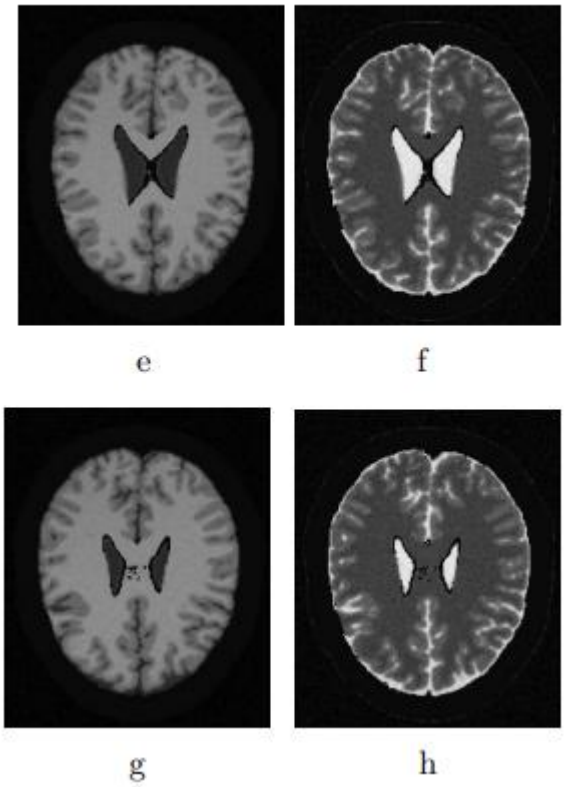

Figure 3.1: In the top row, we have a T1-weighted picture (a) and a T2-weighted image (b) of the brain taken in the Z85 plane, respectively). Second row displays T1- and T2-weighted pictures of the brain in the Z93 plane. In the third row, (e) T1-weighted photos (f) T2-weighted images from a brain MRI taken in the Z96 plane are shown. The fourth row displays the T1- and T2-weighted MRI of the brain in the Z100 plane.

The experimental results show that proposed approach (except for the KSSCM method in certain cases) takes longer to execute than other techniques. The kernel function and spatial limitations from neighboring pixels in clustering process make the suggested approach slower than existing methods. Compared to standard MRI brain tissue segmentation techniques, the proposed approach was more accurate but took longer.

V. Conclusion

MRI brain tissue segmentation finds issues early. Ambiguity, overlap, and fuzzy borders make brain MRI tissue segmentation problematic. Additionally, tissue may stick together. Brain MRI noise may affect segmentation. Chapter 3 extends Chapter 2's RFCMSC by employing the kernel technique to solve brain tissue areas' non-linear separability difficulties to present a resilient kernelized rough fuzzy C-means clustering with spatial restrictions

(KRFCMSC) for brain tissue segmentation from MRI For grouping brain MRI areas with ambiguity, indiscernibility, vagueness, and overlap, use the rough and fuzzy set. Pixels in nonlinear brain tissue are projected into higher dimensions using the kernel approach to improve linear separability. Geographic limits reduce clustering noise and outliers by giving context. Real and synthetic BrainWeb benchmark brain MRI datasets have been utilized in noise-free and noisy investigations. Results include segmentation accuracy (SA), recall, precision, micro and macro averaged F1 measures, Jaccard, dice, Kappa, and kernelized Xie-Beni index. The suggested brain tissue segmentation method is compared to FCM, RFCM, FCMSC, KRFCM, and KSSCM. The proposed MRI brain tissue segmentation approach is more durable and superior than previous methods. The method outperforms alternatives in t-tests and Box-plots.

VI. References

[1] M. C. Wittrock. The Brain and Psychology. Elsevier, Academic Press, United States, first edition, 1980.

[2] T. W. Vanderah and D. J. Gould. Nolte's The Human Brain: An Introduction to its Functional Anatomy. Elsevier, United States, seventh edition, 2015.

[3] Mayfield Education & Research Foundation. Anatomy of the brain. http: //www.mayfieldclinic.com/pe-anatbrain.htm. Accessed: 24 March 2020.

[4] L. M. Biga, S. Dawson, A. Harwell, R. Hopkins, J. Kaufmann, M. LeMaster, P. Matern, K.M. Graham, D. Quick, and J. Runyeon. Anatomy & physiology. https://openstax.org/details/books/ anatomy-and-physiology. Accessed: 24 March 2020.

[5] Prasadu Peddi (2015) "EXPLORING THE IMPACT OF DATA MINING AND MACHINE LEARNING ON STUDENT PERFORMANCE", International Journal of Emerging Technologies and Innovative Research, ISSN:2349-5162, Vol.1, Issue 6, page no. pp314-318, November-2014, Available at : http://www.jetir.org/papers/JETIR1701B47.pdf

[6] Johnson & Johnson Institute. Anatomy & physiology of the brain. https://jnjinstitute.com/sites/default/files/2019-03/092892-181219-Anatomy-Physiology-of-the-Brain.pdf. Accessed: 24 March 2020.

[7] N. P. Alazraki, M. J. Shumate, and D. A. Kooby. A Clinicians Guide to Nuclear Oncology. Society of Nuclear Medicine and Molecular Imaging, Reston, first edition, 2007.

[8] U. S. Department of Health National Cancer Institute and Human Services. Brain tumor. https://www.cancer.gov/types/brain. Accessed: 24 March 2020.

[9] Mayo Foundation for Medical Education Mayo Clinic and Research (MFMER). Brain tumor. https://www.mayoclinic. org/diseases-conditions/brain-tumor/symptoms-causes/ syc-20350084. Accessed: 24 March 2020.

[10] B. W. Stewart and C. P. Wild. World Cancer Report, chapter Tumours of the nervous systems. World Health Organization, 2014.

[11] Alzheimer's Association. Basics of alzheimer's disease. Technical report, Chicago. https://www.alz.org/alzheimer s dementia.

[12] Mayo Foundation for Medical Education Mayo Clinic and Research (MFMER). Alzheimer's disease. https://www.mayoclinic.org/ diseases-conditions/alzheimers-disease/symptoms-causes/ syc-20350447. Accessed: 24 March 2020.

[13] Prasadu Peddi (2015) "A machine learning method intended to predict a student's academic achievement", ISSN: 2366-1313, Vol 1, issue 2, pp:23-37.

[14] L. V. Kalia and A. E. Lang. Parkinson's disease. The Lancet, 386(9996):896–912, 2015.